



Modeling the effect of deep traps on the capacitance–voltage characteristics of p-type Si-doped GaAs Schottky diodes grown on high index GaAs substrates

Nouredine Sengouga^{a,*}, Rami Boumaraf^a, Riaz H. Mari^b, Afak Meftah^a, Dler Jameel^c, Noor Al Saqri^c, Mohsin Azziz^c, David Taylor^c, Mohamed Henini^c

^a Laboratory of Metallic and Semiconducting Materials, Université de Biskra, B.P. 145, 07000 Biskra RP, Algeria

^b Institute of Physics, University of Sindh, Jamshoro, Pakistan

^c School of Physics and Astronomy, Nottingham Nanotechnology and Nanoscience Center, University of Nottingham, Nottingham NG7 2RD, UK

ARTICLE INFO

Keywords:

High index GaAs

Negative differential capacitance: deep levels

SILVACO simulation

ABSTRACT

Numerical simulation, using SILVACO-TCAD, is carried out to explain experimentally observed effects of different types of deep levels on the capacitance–voltage characteristics of p-type Si-doped GaAs Schottky diodes grown on high index GaAs substrates. Two diodes were grown on (311)A and (211)A oriented GaAs substrates using Molecular Beam Epitaxy (MBE). Although, deep levels were observed in both structures, the measured capacitance–voltage characteristics show a negative differential capacitance (NDC) for the (311)A diodes, while the (211)A devices display a usual behaviour. The NDC is related to the nature and spatial distribution of the deep levels, which are characterized by the Deep Level Transient Spectroscopy (DLTS) technique. In the (311)A structure only majority deep levels (hole traps) were observed while both majority and minority deep levels were present in the (211)A diodes. The simulation, which calculates the capacitance–voltage characteristics in the absence and presence of different types of deep levels, agrees well with the experimentally observed behaviour.

© 2015 Elsevier Ltd. All rights reserved.

1. Introduction

Silicon (Si) doping of Gallium Arsenide (GaAs) and other III–V semiconductors offers an advantage over Beryllium (Be) because of its amphoteric nature. It can be either a donor (occupies a group V site) or acceptor (occupies a group III site) depending on the substrate orientation [1–5]. Si is mainly a donor when the growth is on the (100) surface. However, silicon incorporates preferentially as a donor in (N11)B, and as an acceptor or a donor on (N11)A surfaces (N=1,2,3) depending on the substrate temperature and the arsenic overpressure used during the MBE growth. A and B

denote a Ga- and As-terminated plane, respectively. Thus, the interest in the growth of III–V compound semiconductors on high index planes, other than the conventional (100) orientation, has increased tremendously over the last several years. In fact the MBE growth of p-type GaAs/AlGaAs heterostructures on (311)A results in higher hole mobilities than those based on the conventional Be-doped p-type on (100) GaAs plane [6–11]. A wide variety of structures can be grown on high index planes such as quantum wire structures [12], quantum dots [13,14], zero-dimensional quantum dots and one-dimensional quantum wires [15–17].

The growth of semiconductor layers and structures strongly depends on the substrate orientation and hence to surface atomic arrangement [18,19]. This may lead to some defects which could have deleterious effects on the electrical and optical properties of III–V based devices [20].

* Corresponding author.

E-mail address: n.sengouga@univ-biskra.dz (N. Sengouga).

For example a negative capacitance (NC) is frequently observed in the capacitance–voltage characteristics in structures where deep traps are present. For example, Jones et al. [21] reported a forward bias negative capacitance, and Saadouné et al. [22] used numerical simulation to relate the NC to defects in the semiconductor diodes subjected to high fluence of energetic particles. Yahia et al. [23] and Korucu et al. [24] related this effect to interface states and series resistance. The so-called negative differential capacitance (NDC) is another effect due to the presence of deep levels. Stuchlíková et al. [25] observed that NDC increases with increasing temperature and is a characteristic of quantum well heterostructures. Kumar et al. [26] also argued that NDC is the result of free electron emission from quantum states. Simulation of a three layered GaAs structure showed that the presence of deep levels produces a NDC effect [27]. Silicon implantation of GaN P-I-N photodetectors also showed a NDC behaviour, which increases with increasing temperature [28]. It is argued that this is due to defects introduced by implantation. A study of the effect of temperature on the electrical characteristics of GaAsN Schottky diodes revealed an apparent high density of traps [29].

In this work two Si doped p-type GaAs samples were grown by Molecular Beam Epitaxy (MBE) on (211)A and (311)A oriented GaAs semi-insulating substrates, named hereafter NU928 and NU926, respectively. They are investigated using capacitance–voltage (C–V) measurements at different temperatures and Deep Level Transient Spectroscopy (DLTS). Although DLTS measurements revealed the existence of several deep levels in each structure, the C–V characteristics are entirely different. In NU928, the C–V characteristics have the usual shape for all temperatures and increase monolithically. In NU926, however, the C–V characteristics begin with the usual shape for low temperatures. As the temperature increases the C–V characteristics deviate from the usual shape and NDC manifests clearly. The difference in the shape of the C–V characteristics is related to the difference in the deep levels observed in the two samples. In order to relate the C–V shape to the observed deep levels, the SILVACO-TCAD software is used to calculate these characteristics of the two samples [30]. The experimental and simulation data are then compared.

2. Experimental details

p-type Si-doped GaAs samples are grown on (N11)A (N=2,3) planes to investigate the electrical properties and the defects present in epitaxial layers grown on different Miller indices. They were characterized by C–V and DLTS techniques.

2.1. Samples

Sample NU926 is grown on semi-insulating (311)A GaAs substrate. It consists of a 0.1 μm undoped GaAs buffer layer followed by a 0.5 μm Si-doped p-type GaAs layer. Further details about the growth of these samples can be found in our previous work [31].

2.2. Capacitance–voltage measurements

The analysis of the C–V characteristics provides important parameters such as the built-in voltage, the background doping concentration and concentration depth profile. The DLTS data analysis relies on these parameters. Therefore, C–V characteristics of each device are measured using a BOONTON 7200 Capacitance Meter, which is controlled by a computer. It operates at a frequency of 1 MHz.

2.3. DLTS and Laplace DLTS measurements

DLTS and Laplace DLTS are used as the main tool for the characterization of deep levels present in the material systems. The samples packaged in a TO5 header were mounted on a sample holder. The samples were first cooled down to a temperature of 10 K in a Closed Cycle Cryodyne Refrigerator, model number CCS-450. DLTS measurements were then started by ramping the temperature at a rate of 2 K/min. A train of electrical pulses, generated by a pulse generator (model Agilent 33220A) was applied to the samples. The filling pulse repetition rate is fixed to 50 Hz. The reverse bias (VR) and filling pulse (VP) is applied in such a way that $VP < VR$.

For the resolution of the broad featureless DLTS peaks, High Resolution Laplace DLTS measurements were carried out. Laplace DLTS is an isothermal DLTS process, where the measurements are performed at constant temperature within a temperature range where the conventional DLTS peak appears. Further details of the measurements can be found in [32].

3. The simulation software SILVACO-TCAD

In order to characterize semiconductor devices and relate the observed effects to each other, extensive experimental work has to be carried out. In some cases, analytical or qualitative modelling has to be used to relate these experimentally observed effects. The experimental characterization turns out to be time consuming and can be very expensive. The analytical modelling has to accept several simplifications. Numerical simulation is an alternative and a powerful tool. Many parameters can be varied to model the observed phenomenon. In this present study the variables are the defects and the phenomenon is the capacitance–voltage characteristics evolution with temperature. Numerical simulation can also offer a physical explanation of the observed phenomenon since internal parameters can be calculated such as the electrical field and the free carrier densities.

SILVACO (Silicon Valley Company) is a commercial software which consists of several modules including ATLAS [30]. ATLAS is a physically based two- and three-dimensional semiconductor device simulator. It predicts the electrical behaviour associated with the physical structure under specified biased conditions (DC, AC, transient, frequency dependence, etc...). ATLAS achieves this through partitioning the specified device into a two or three-dimensional mesh grid. ATLAS then applies a set of differential equations, based on Maxwell's Laws, to the mesh to simulate the transport of carriers through the structure. These equations consist of the well known Poisson's equation, the carrier continuity equations and the transport

equations. Further details can be found in our previous work [31].

Of interest to the present work, the capacitance–voltage characteristics are calculated under different conditions (presence or absence of deep levels) at various temperatures. In this work, the capacitance–voltage characteristics are calculated for different types of deep levels and compared to experiments.

4. Results and discussions

4.1. Measurements

First the capacitance–voltage characteristics are measured at different temperatures ranging from 20 to 300 K for the two samples. Typical examples are shown in Fig. 1 and Fig. 2 for the samples NU926 and NU928 respectively. The C–V characteristics for only three temperatures are presented to avoid curve overcrowding. However, these three temperatures are representative of others as can be verified in the full plot in our previous paper [31].

The NU928 C–V characteristics have the usual shape characterized by the proportionality $C \propto 1/\sqrt{(V_B + |V_R|)}$ where V_B and V_R are the Schottky barrier height and the

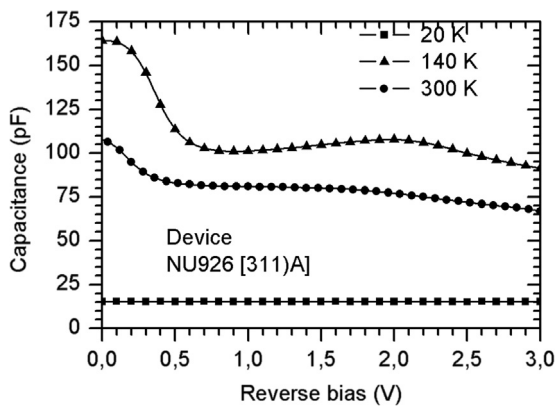


Fig. 1. The capacitance–voltage characteristics at different temperatures for the sample NU926 [(311)A].

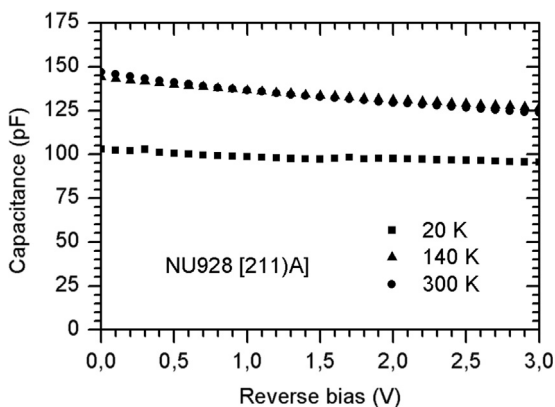


Fig. 2. The capacitance–voltage characteristics at different temperatures for the sample NU928 [(211)A].

reverse voltages, respectively. However, the NU926 sample characteristics have a more complicated shape and are more affected by the temperature. It is evident that for this sample the C–V curve departs from the conventional shape. In fact they show negative differential capacitance (NDC) behaviour. The difference between the C–V characteristics can be explained by the presence of different types of deep levels in the two structures. Typical DLTS spectra are presented in Fig. 3. The filling pulse has a height of 0.8 V, a reverse bias of -0.5 V and a filling time of 1 ms. The rate window employed is 200 Hz. The negative peak is due to majority deep levels (hole deep levels in this case) while the positive one represents minority deep levels (electron deep levels). For sample NU926, only majority (hole) deep levels are found while both hole and electron deep levels are detected in NU928. It is worth pointing out that there is a difference in the scales of DLTS signals for the two samples. The electron deep level in NU928 has a DLTS signal about 40 times larger than the hole deep levels. Therefore, the positive DLTS signal (signature of electron deep levels) is divided by a factor of 20 so that the negative signal (hole deep levels) can be clearly seen. The real scale is shown in the inset. This means that the electron deep levels have a much higher density than hole deep levels. These are the main reasons (different types of deep levels and different densities) of the observed difference in the C–V characteristics of the two samples. However at a low temperature the traps are not active so the NDC phenomenon is not observed.

Details of deep levels characterized by DLTS and Laplace DLTS are given elsewhere [31]. They are summarized in Tables 1 and 2 for samples NU926 and NU928, respectively, for convenience. In both tables E and H stand for an electron and hole trap, respectively. The activation energies for electron and hole traps are with regard to the conduction and valence band, respectively.

The relation between the capacitance–voltage characteristics and the presence of defects is first explained qualitatively. As a preliminary analysis one can get a rough estimation of the effective doping profile which can be

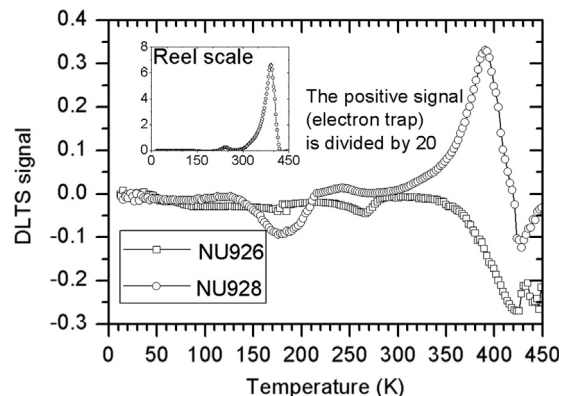


Fig. 3. DLTS spectra for NU926 (circles) and NU928 (squares) samples. For NU928 the positive signal (electron deep levels) is divided by 20. The actual scale of the positive signal is shown in the inset. The filling pulse has a height of 0.8 V, a reverse bias of -0.5 V and a filling time of 1 ms. The rate window employed is 200 Hz.

Table 1
The defect parameters determined by Laplace DLTS for NU926 sample.

Deep level	Activation energy (eV)	Density (cm ⁻³)	Capture cross section (cm ²)
H ₁	0.025 ± 0.003	1.43 × 10 ¹⁵	1.63 × 10 ⁻¹⁸
H ₂	0.014 ± 0.002	1.47 × 10 ¹⁵	4.79 × 10 ⁻¹⁷
H ₃	0.247 ± 0.005	1.19 × 10 ¹⁵	7.35 × 10 ⁻¹⁸
H ₄	0.837 ± 0.007	1.54 × 10 ¹⁵	6.75 × 10 ⁻¹⁸

Table 2
The defect parameters determined by Laplace DLTS for the sample NU928.

Deep level	Activation energy (eV)	Density (cm ⁻³)	Capture cross section (cm ²)
H ₁	0.061 ± 0.014	5.65 × 10 ¹⁵	5.35 × 10 ⁻¹⁶
H ₂	0.075 ± 0.011	6.64 × 10 ¹⁵	4.36 × 10 ⁻¹⁶
H ₃	0.153 ± 0.03	2.81 × 10 ¹⁵	4.36 × 10 ⁻¹⁶
H ₄	0.170 ± 0.02	3.39 × 10 ¹⁵	4.77 × 10 ⁻¹⁶
H ₅	0.283 ± 0.001	7.83 × 10 ¹⁴	3.99 × 10 ⁻¹⁶
E	0.431 ± 0.019	1.68 × 10 ¹⁶	3.33 × 10 ⁻¹⁷

extracted from the C–V characteristics using the following formula [33,35]:

$$N_{eff}(W \text{ or } V) = 2 \cdot \frac{dV}{d(1/C^2)} \cdot (eA^2 \epsilon_r \epsilon_0)^{-1} \quad (1)$$

A is the diode cross section, W is the depletion region width. The other symbols have the usual meaning [33]. A typical example is shown in Fig. 4 for NU928 and NU926 samples at 300 K. The average effective density is ~ 6.0 × 10¹⁶ and ~ 2.2 × 10¹⁶ cm⁻³ for NU928 and NU926 samples, respectively. A peak appears at a depth of ~ 0.4 μm in the NU926 sample. It will be shown later (by simulation) that this peak is related to a defect which manifests itself as a deep acceptor and is the cause of the NDC behaviour.

Let us first consider the capacitance of a p-type Schottky diode. In the absence of defects, it is given by the well-known formula for a uniform and abrupt distribution of impurities [34]:

$$C = \sqrt{\frac{q \cdot \epsilon_s \cdot N_A^-}{2(V_B - V - \frac{k \cdot T}{q})}} \quad (2)$$

N_A⁻ is the ionized acceptor doping density and V_B is the Schottky barrier voltage. In the presence of defects, the capacitance formula should be modified to take into account these changes. Thus

$$C = \sqrt{\frac{q \cdot \epsilon_s \cdot (N_A^- \mp \sum N_{Ti}^{\mp})}{2(V_B - V - \frac{k \cdot T}{q})}} \quad (3)$$

where N_{Ti}[±] is the ionized *i*th deep level (the sign indicates whether it is a donor or acceptor). It should be mentioned here that Eq. (3) is only valid for a uniform distribution of deep levels. Otherwise the C–V characteristics will depart from this usual shape. It seems in the present case that sample NU928 has a uniform distribution of dopants and

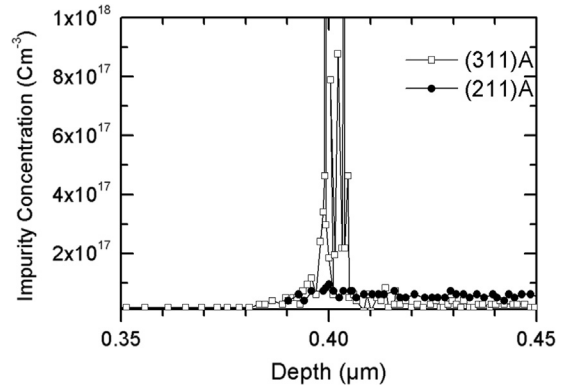


Fig. 4. The effective density profile evaluated from the C–V characteristics of the NU928 and NU926 samples at 300 K.

deep levels while NU926 has a non-uniform distribution of either the doping density or deep levels. This is what will be clarified using simulation.

4.2. Simulation

In order to relate the observed different C–V characteristics of the two samples to the presence of deep defects, a simulation of two structures using SILVACO-TCAD is carried out. The two structures are similar but they differ only in the defects introduced. The parameters, other than the defects, are those described in Section 2.1. The first structure includes only deep acceptors as in the case of NU926. The second structure incorporates both deep donors and acceptors as in the case of NU928.

In carrying out numerical simulation, it has to be mentioned that there are several different parameters to adjust in order to fit the measurements. These include type of defect and its properties (activation energy, capture cross section and density), and other parameters of the material (e.g. mobility, lifetime, doping density, etc). Therefore numerical simulation is usually more difficult than analytical modelling because of the reasons mentioned above. In the latter, much fewer parameters have to be adjusted and in most cases they do not have a physical meaning. In this work the activation energy of deep levels are fixed (Tables 1 and 2) while their density and/or their profile is varied to set the simulation as close as possible to measurements.

4.2.1. Sample NU926

For this sample, DLTS reveals four majority deep levels and the C–V characteristics show NDC behaviour. Fig. 3 shows that the effective doping density profile, evaluated from the C–V characteristics, is not uniform. Therefore in simulating this sample we will suppose that only one level has a non-uniform profile while all others are uniformly distributed. This includes also the doping of the shallow level (shallow dopant impurity). The different cases are shown in Fig. 5 at 300 K. The densities of the levels with uniform profile are those of Table 1. The non-uniform level has a narrow Gaussian with a standard deviation of 0.003 μm while the peak density and position are variables

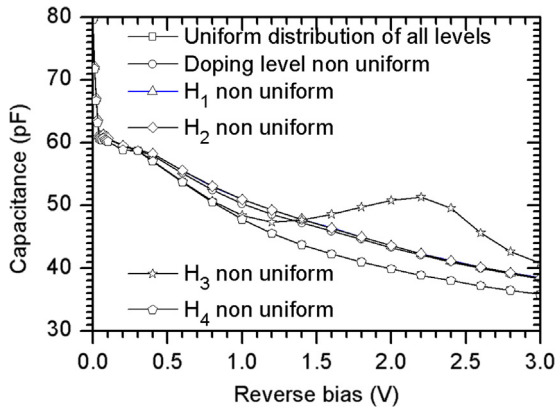


Fig. 5. The simulated capacitance–voltage characteristics of NU926 sample for non-uniform distribution of different traps at 300 K.

until the NDC is obtained. In Fig. 5 the peak density is $1.0 \times 10^{18} \text{ cm}^{-3}$ at $0.418 \mu\text{m}$ from the Schottky contact.

It is clear that only a non-uniform distribution of the deep level H_3 produces NDC. To further investigate this we have simulated the effect of the H_3 density on the C – V characteristics, which is shown in Fig. 6. Small values of H_3 density ($< 10^{17} \text{ cm}^{-3}$) do not show NDC. As this density increases a NDC is observed and increases with the concentration. As the density reaches 10^{19} cm^{-3} , NDC disappears.

Further evidence of the responsibility of H_3 for the NDC is provided by the simulation of the effect of the position of the density peak from the surface on the C – V characteristics, as presented in Fig. 7. For a distance of $0.3 \mu\text{m}$ from the surface, a large NDC can be seen but the peak is very narrow and does not resemble experimental observation. For $0.4 \mu\text{m}$, although NDC is present but it persists over a wide range of voltage (from 1 to $> 3 \text{ V}$). For other positions, NDC is not observed at all except for $0.418 \mu\text{m}$. In fact even a negative capacitance is observed as shown in the inset of Fig. 6. This phenomenon was studied previously [22]. The position of $0.418 \mu\text{m}$ is very similar to that observed experimentally (Fig. 4). The effect of any trap on the C – V characteristics will be observed only if its energetic position changes with respect to the Fermi level and this can only occur in a depletion region. In the present case if the depletion region edge does not reach the trap position then this trap will have no effect. Finally it has to be mentioned that in this work we were not interested in reproducing the capacitance value as much as elucidation the NDC phenomenon. Why does it appear in one sample and not in the other?

4.2.2. Sample NU928

For this sample, DLTS reveals both majority and minority deep levels. The C – V characteristics show the usual shape but with a slow changing capacitance with reverse bias. Fig. 4 shows that the effective doping density profile, evaluated from the C – V characteristics, is uniform. In simulating the C – V characteristics of this sample we will use uniform distribution of all levels (doping and deep) and use the values given in Table 2. However, the C – V characteristics do not resemble the measured capacitance.

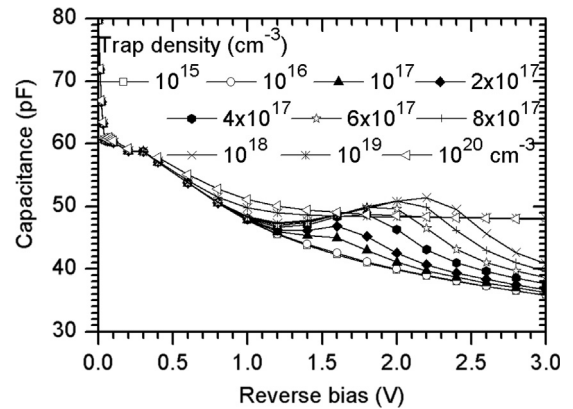


Fig. 6. The simulated capacitance–voltage characteristics of the NU926 sample for different densities of the non-uniformly distributed H_3 . Other levels are kept uniform.

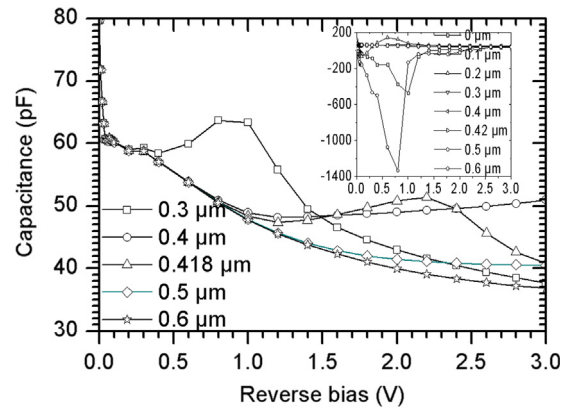


Fig. 7. The simulated capacitance–voltage characteristics of the NU926 sample for different positions of the non-uniformly distributed H_3 from the surface. The inset is for other positions for which a negative capacitance appears.

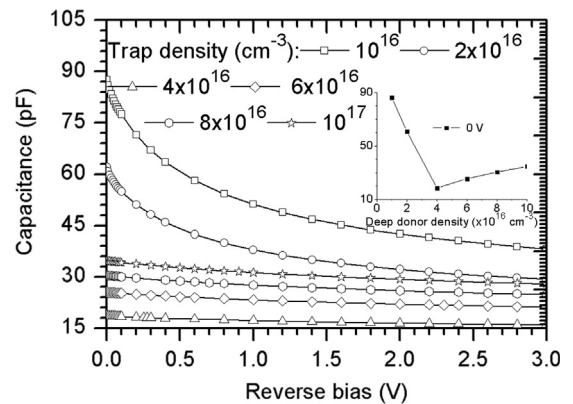


Fig. 8. The simulated capacitance–voltage characteristics of the NU928 sample for different densities of the deep donor level E . The inset is the capacitance for a bias of 0 V versus the deep donor density showing the type conversion phenomenon at 300 K.

To get comparable simulation and measurement, the C – V characteristics were simulated for different deep donor density. The simulation results at 300 K are shown in

Fig. 8. The measured C–V characteristic is reproduced for a deep donor density of $\sim 4 \times 10^{16} \text{ cm}^{-3}$ which is a bit higher than that given in Table 2. This may be due to the value of the acceptor doping density used in the simulation which may be not correct.

An interesting phenomenon is observed in this simulation. The capacitance (at any bias) decreases with increasing density of the deep donor level then increases after the latter surpasses a value of $\sim 4 \times 10^{16} \text{ cm}^{-3}$ as shown in the inset of Fig. 8 for a bias of 0 V. This is the value of the deep donor density where simulation is comparable to measurement. The decrease and increase of the capacitance with increasing density of deep levels is a well-known phenomenon and is usually attributed to a type conversion of the semiconductor [35]. In the present case the p-type semiconductor has become n-type because of the high density of the deep donor.

5. Conclusion

Two p-type silicon-doped GaAs Schottky diodes grown on (311)A and (211)A Si GaAs substrates were characterized by capacitance–voltage, capacitance–temperature and DLTS measurements. The capacitance–voltage characteristics of the (311)A sample were found to depart from the usual C–V dependence. DLTS revealed that in the (311)A sample only majority type defects are present, while in the (211)A sample both majority and minority related defects were detected. The departure of the C–V characteristics was related to the presence of a deep acceptor defect which has a non-uniform density. Numerical simulation by the SILVACO-TCAD software was successfully used to reproduce the experimentally observed effects.

References

- [1] R.H. Mari, M. Shafi, M. Henini, D. Taylor, *Phys. Status Solidi C* 6 (2009) 2873.
- [2] L. Pavesi, Nguyen Hong Ky, J.D. Ganière, F.K. Reinhart, N. Baba-Ali, I. Harrison, B. Tuck, M. Henini, *J. Appl. Phys.* 71 (1992) 2225.
- [3] W.I. Wang, E.E. Mendez, T.S. Kuan, L. Esaki, *Appl. Phys. Lett.* 47 (1985) 826.
- [4] B. Lee, S.S. Bose, M.H. Kim, A.D. Reed, G.E. Stillman, W.I. Wang, L. Vina, P.C. Colter, *J. Cryst. Growth* 96 (1989) 27.
- [5] I. Harrison, L. Pavesi, M. Henini, D. Johnston, *J. Appl. Phys.* 75 (1994) 3151.
- [6] R.H. Mari, M. Shafi, M. Aziz, A. Khatab, D. Taylor, M. Henini, *Nanoscale Res. Lett.* 6 (2011) 180.
- [7] A.G. Davies, R. Newbury, M. Pepper, J.E.F. Frost, D.A. Ritchie, G.A.C. Jones, *Phys. Rev. B* 44 (1991) 13128.
- [8] A.G. Davies, R. Newbury, M. Pepper, J.E.F. Frost, D.A. Ritchie, G.A.C. Jones, *Surf. Sci.* 263 (1992) 81.
- [9] M.B. Santos, J. Yo, Y.W. Suen, L.W. Engel, M. Shayegan, *Phys. Rev. B* 46 (1992) 13639.
- [10] J.J. Heremans, M.B. Santos, M. Shayegan, *Appl. Phys. Lett.* 61 (1992) 1652.
- [11] M. Henini, P.J. Rodgers, P.A. Crump, B.L. Gallagher, G. Hill, *Appl. Phys. Lett.* 65 (1994) 2054. 16.
- [12] V.R. Yazdanpanah, Z.M. Wang, G.J. Salamo, *Appl. Phys. Lett.* 82 (2003) 1766.
- [13] G.E. Dialynas, S. Kalliakos, C. Xenogianni, M. Androulidaki, T. Kehagias, P. Komninou, P.G. Savvidis, Z. Hatzopoulos, N.T. Pelekanos, *J. Appl. Phys.* 108 (2010) 103525.
- [14] S. Sanguinetti, M. Gurioli, M. Henini, *Microelectron. J.* 33 (2002) 583.
- [15] H. Wen, Z.M. Wang, G.J. Salamo, *Appl. Phys. Lett.* 84 (2004) 1756.
- [16] Z. Li, J. Wu, Z.M.W.D. Fan, A. Guo, S. Li, S.Q. Yu, O. Manasreh, G. J. Salamo, *Nanoscale Res. Lett.* 5 (2010) 1079.
- [17] T. Kawazu, *Physica E* 44 (2012) 1351.
- [18] J. Ibáñez, R. Kudrawiec, J. Misiewicz, M. Schmidbauer, M. Henini, M. Hopkinson, *J. Appl. Phys.* 100 (2006) 093522.
- [19] M. Henini, O.Z. Karimov, G.H. John, R.T. Harley, R.J. Airey, *Phys. E: Low-dimens. Syst. Nanostruct.* 23 (2004) 309.
- [20] M. Shafi, R.H. Mari, A. Khatab, D. Taylor, M. Henini, *Nanoscale Res. Lett.* 5 (2010) 1948.
- [21] B.K. Jones, J. Santana, M. McPherson, *Solid State Commun.* 107 (1998) 47.
- [22] A. Saadoun, L. Dehimi, N. Sengouga, M. McPherson, B.K. Jones, *Solid-State Electron.* 50 (2006) 1178.
- [23] I.S. Yahia, G.B. Sakr, S.S. Shenouda, M. Fadel, S.S. Fouad, F. Yakuphanoglu, *Appl. Phys. A* 112 (2013) 275.
- [24] D. Korucu, A. Turut, S. Altındal, *Curr. Appl. Phys.* 13 (2013) 1101.
- [25] L. Stuchlíková, L. Harmatha, M. Petrus, J. Rybár, J. Šebok, B. Šciana, D. Radziewicz, D. Pucicki, M. Hłaczala, A. Kósa, P. Benko, J. Kováš, P. Juhász, *Appl. Surf. Sci.* 269 (2013) 175.
- [26] M. Kumar, T.N. Bhat, M.K. Rajpalke, B. Roul, N. Sinha, A.T. Kalghatgi, S.B. Krupanidhin, *Solid State Commun.* 151 (2011) 356.
- [27] S.A. Kostylev, E.F. Prokhorov, N.B. Gorev, I.F. Kodzheshpirov, Y.A. Kovalenko, *Solid-State Electron.* 43 (1999) 169.
- [28] X. Bao, J. Xu, C. Li, H. Qiao, Y. Zhang, X. Li, *J. Alloy. Compd.* 581 (2013) 289.
- [29] B. Bouzazi, N. Kojima, Y. Ohshita, M. Yamaguchi, *J. Alloy. Compd.* 552 (2013) 469.
- [30] SILVACO-TCAD, ATLAS User's Manual: Device Simulation Software, Silvaco International, California, 2004.
- [31] R. Boumaraf, N. Sengouga, R.H. Mari, A.F. Meftah, M. Aziz, Dler Jameel, Noor Al Saqri, D. Taylor, M. Henini, *Superlattices Microstruct.* 65 (2014) 319.
- [32] R.H. Mari, *Electrical Characterisation of Defects in III–V Compound Semiconductors by DLTS* (Ph.D. thesis) University of Nottingham, 2011.
- [33] S.E. Laux, *IEEE Trans. Electron Devices* 32 (1985) 2028.
- [34] S.M. Sze, *Physics of Semiconductor Devices*, 2nd ed. John Wiley, New York, 1982.
- [35] A. Saadoun, S.J. Moloi, K. Bekhouche, L. Dehimi, M. McPherson, N. Sengouga, B.K. Jones, *IEEE Trans. Device Mater. Reliab.* 13 (2013) 1.